Study of the structure of $MgSiO_3$ system under compression by using ring statistics and voronoi analysis

Physica Scripta

PAPER

Study of the structure of $MgSiO_3$ system under compression by using ring statistics and voronoi analysis

Hoang Anh Nguyen[1,2,*] **and Nguyen Van Hong**[1]

[1] Hanoi University of Science and Technology, Hanoi 100000, Vietnam
[2] International Center for Theoretical Physics, Trieste 34151, Italy
[*] Author to whom any correspondence should be addressed.

E-mail: hoanganhnguyen.vietnam@gmail.com

Keywords: $MgSiO_3$ liquid, ring statistics, Mg-rich region, Voronoi, second peak splitting

OPEN ACCESS

RECEIVED
21 July 2022

REVISED
26 February 2023

ACCEPTED FOR PUBLICATION
20 March 2023

PUBLISHED
30 March 2023

Abstract

The structural change of $MgSiO_3$ liquid under compression is still one of the most interesting challenges. In this paper, we perform the molecular dynamics simulation to study the structural change of $MgSiO_3$ liquid from 0 to 200 GPa. Ring statistics are analyzed to clarify the intermediate-range order, to explain why the second peak of Si–Si PRDFs splits into 2 subpeaks at 200 GPa, and to show the heterogeneity of $MgSiO_3$. Large rings which form at high pressures would capture the oxygen atoms. Oxygen atoms which have negative charge attract Mg^{2+} ions, creating magnesium-rich regions. Besides, the Voronoi and Q^n distribution changes on the ring with pressure are clarified to give more information about the rings.

1. Introduction

The magnesium silicate system is one of the main components of the Earth's mantle, chondrite meteorites and interplanetary dust [1–3]. It also plays an important application in technological and scientific fields such as materials science or geoscience. Therefore, it is necessary to study the structural properties of this material at different physical conditions. The continuous silicate network is mainly constructed by SiO_4 units through corner linkages. Adding MgO leads to the reduction of the polymerization of -Si–O- network and the formation of non-bridging oxygens (NBOs) and free oxygens (FOs). In $MgSiO_3$, Mg can act as both network former and network modifier [4–6]. Previous works state that there are structural changes in the MgO-SiO_2 system by compression [7–9], by the molar ratio of MgO/SiO_2 content [10] and by temperature changing [11–13].

The radial distribution function and coordination number are among typical criteria for evaluating the local structure of materials. The average Si–O bond length in both $MgSiO_3$ glass and liquid is about 1.66 Å and does not depend much on temperature [14, 15]. Under mild compression, the mean bond lengths of Si-O and Mg–O increase slightly [13, 16]. The first peak of Si–O pair radial distribution functions (PRDF) shifts from 1.64 Å at 0 GPa to 1.68 Å at 30 GPa and the one of Mg–O PRDF shifts from 1.98 Å to 2.02 Å [17]. From neutron, x-ray diffraction data and a reserve Monte Carlo (RMC) simulation, authors in previous work suggested that Mg–O bond length has two values of 1.99 ± 0.01 and 2.21 ± 0.01 Å and Mg–O correlation is skewed to the high-r side [18]. Also by x-ray diffraction, M. Wilding *et al* indicate that the coordination number of Si–O is 4.0 while the one of Mg–O is 4.5 ± 0.2 due to the mixture of MgO_x with $x = 4, 5, 6$ [10]. In particular, the fraction of MgO_4, MgO_5 and MgO_6 is 68.8%, 27.8% and 3.4% respectively [18, 19].

The intermediate-range order (IRO) is related to the connection of polyhedrons. There is no clear boundary between short and intermediate-range order. The IRO is usually considered relevant from 3 to 10 Å, that is $\sim 2\pi/Q_{First\ Sharp\ Diffraction\ Peak}$ [20]. The SiO_x polyhedrons bond to others by corner-, edge- and face-sharing linkages. The number of these linkages strongly change under compression [21–24]. At low pressure, the polyhedrons are connected mainly through corner-sharing linkages. When the pressure increases, edge- and face-sharing linkages are created, participating in the network formation. The same goes for Mg-Si pairs. The formation of face-sharing bonds has resulted in unequal density distribution and heterogeneity in the material

Table 1. The first peak position of radial distribution functions (PRDFs) in $MgSiO_3$ liquid, at 0 GPa.

	First peak position (Å)			Coordination number	
	Si–O	O–O	Mg–O	Si	Mg
This study	1.64	2.68	1.96	4.1	4.5
J Haskins *et al* [12]	1.6	—	2.1	4.0	5.0
M Wilding *et al* [40]	1.64	2.64	2	4.0	4.5
Y Matsui and K Kawamura [41]	1.62	2.65	1.96	—	—
L T San *et al* [17]	1.64	2.56	1.98	—	4.3

[14, 17, 25]. The existence of Mg-rich regions under pressure is analyzed through the number of FO atoms and the formation of OMg_x clusters [26]. In this paper, we carry out a different approach to the analysis of Mg-rich regions, which is to use ring statistics. Although ring statistics has been studied extensively in SiO_2 and $MgSiO_3$ glass [24, 27–32], studies on rings in $MgSiO_3$ liquid have been still in question.

The network information such as IRO [18] or the degree of polymerization [33] can be examined by the Q^n species, in which, n is the number of bridging oxygens (BOs). In $MgSiO_3$ glass, the distribution of Q^n units changes as a function of pressure [26]. In particular, when pressure rises up, the number of Q^n, with $0 \leqslant n \leqslant 2$, decreases while the number of Q^n, with $3 \leqslant n \leqslant 6$, increases. In $MgSiO_3$ liquid, however, the Q^n distribution under compression, especially the Q^n distribution on rings, has not been studied in detail. Therefore, in order to see the connectivity characteristic of rings into the network, we analyze the Q^n distribution of SiO_x units on different types of rings (here, n is still the number of BOs of SiO_x units).

In terms of Voronoi, by RMC modelling and density function theory (DFT) simulation, previous work shows that the Voronoi volumes of Mg are greater than Bader volumes [34]. In $MgSiO_3$ glass, the Mg-Voronoi volume is about 13.36 Å for the RMC model and 12.69 Å for the DFT model. In Mg_2SiO_4, these values decrease to 11.83 Å and 12.52 Å, respectively. There have been some works on Voronoi in $MgSiO_3$, however, the Voronoi analysis on rings in this material has not been clarified yet.

In this work, 5000-atom $MgSiO_3$ liquid models from 0 to 200 GPa are built by molecular dynamics simulation. We analyze the local structural change under pressure of the material through radial distribution function and coordination number. The Si–O ring statistics is clarified to explain the second peak splitting of the Si–Si radial distribution function at 200 GPa and the formation of Mg-rich regions under pressure. Q^n and Voronoi are analyzed to provide additional information on rings. The article is arranged according to the layout: section 2 is simulation method, section 3 is the result and discussion, section 4 is the conclusion.

2. Methodology

Pressure-induced $MgSiO_3$ liquid models are erected by molecular dynamics simulation. Each model contains 5000 atoms (1000 Si, 3000 O and 1000 Mg atoms) with the periodic boundary condition. The temperature of the model is 3000 K and pressure is in the range from 0 to 200 GPa. The Oganov potential which is applied is presented as:

$$\varphi_{ij}(r_{ij}) = \frac{q_i q_j e^2}{4\pi r_{ij}} + A_{ij}\exp\left(-\frac{r_{ij}}{B_{ij}}\right) - \frac{C_{ij}}{r_{ij}^6}$$

in which, q_i, q_j are effective charges of atom i and atom j; r_{ij} is the distance between i and j atoms; e is the charge of the electron; A_{ij} and C_{ij} are parameters attributing van de Waals repulsion and attraction, respectively; B_{ij} is an e-folding length characterizing the radially-symmetric decay of electron repulsive Born energy between species i and j [35–38]. We use the Verlet algorithm with the time step of 0.47 fs to run the model. At first, atoms are randomly scattered inside a box and heated up to 6000 K to lose the memory of the initial configuration. The model then is quenched to 3000 K with the cooling rate of 2.5 K/ps. During that process, the model is relaxed at 5000 and 4000 K. At 3000 K, a long relaxation of 10^7 MD time steps is done in the NPT ensemble. The $MgSiO_3$ liquid model at 0 GPa is obtained. Finally, the model is compressed to desired pressures. The physical quantities of each model are analyzed based on averaging data from 1000 last MD steps.

To determine the correlations among atoms, the r_{cut} is chosen based on the position of the first notch after the first peak of the PRDFs and adjusted to specific pressures. In this work, r_{cut} for Si–O pair is 2.50 Å at 0 GPa and, in general, decreases to 2.35 Å at 200 GPa. The first peak positions of Si–O, O–O and Mg–O PRDFs (see appendix - figure A·1) in $MgSiO_3$ liquid at ambient pressure are consistent with previous work and listed in

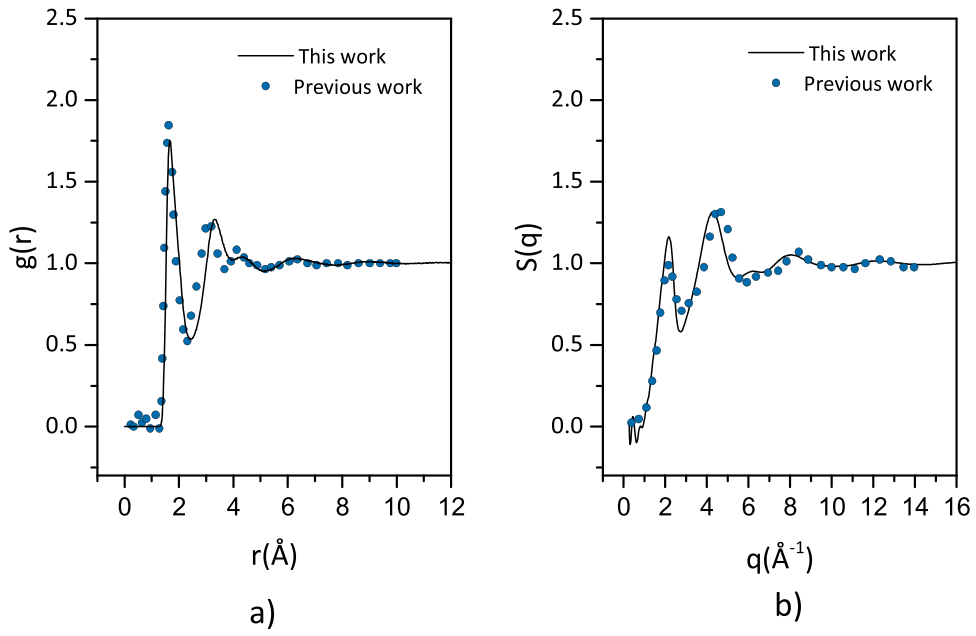

Figure 1. The radial distribution function (a) and structure factor (b) of $MgSiO_3$ at 0 GPa in this work and previous work [39].

table 1.The total radial distribution function (RDF) and the structure factor of $MgSiO_3$ at different pressures are also in good agreement with previous work [39] (see figure 1).

To analyze ring statistics, the -Si–O– network is considered as the undirected graph, whereas each atom is a node. Within the undirected graph, the path is the series of nodes and linkages that are connected consequently without overlap. There are a number of ring definitions. Some typical ring definitions that could be referred to are classic King's criterion [42], the irreducible [43, 44] /primitivity [45, 46]/no shortcut path [47] criterion, the shortest paths criterion [48, 49]. Using different ring definitions could result in different number of rings. In this work, we use the no shortcut path criterion and algorithm which are introduced in the study of M Matsumoto *et al* [47]. *n*-fold ring consists of *n* T atoms (T is Mg or Si) and *n* O atoms. Typical Si rings are displayed in figure 2.

3 Results and discussion

3.1 Structural change under compression

Under compression, the atoms are packed into small domains [20]. Therefore, both the coordination numbers of Si and Mg strongly depend on pressure (see figure 3). At 200 GPa, the coordination numbers of Si and Mg are about 6.8 and 8.4, respectively. Besides, average bond lengths of O–O, Si–Si decrease significantly while Si–O bond length decreases slowly as pressure rises (see figure 4). The first peaks of O–O and Si–Si PRDF shift to the left under pressure, the peak, however, is higher. At 200 GPa, the atoms are arranged in an orderly manner compared to lower pressures as there is a phase transition from the liquid to the solid between 150 and 200 GPa. Especially, the second peak of the Si–Si PRDF splits into two subpeaks at 200 GPa. This will be explained based on ring statistics in the next section. The O–O and Si–Si bonds contract significantly with pressure - from 2.7 Å to 2.22 Å for O–O and from 3.22 Å to 2.8 for Si–Si. This is attributed to the massive formation of SiO_x (x = 5, 6, 7) polyhedrons (see figures 5 and 6). In the course of the pressure-rising process, there increasingly are edge-sharing and face-sharing Si–Si bond linkages in the -Si–O- network. The mean edge-sharing bond length is shorter than the mean corner-sharing one and longer than the mean face-sharing one (see appendix - table A·1). Therefore, the mean Si–Si bond length decreases significantly as pressure rises. In terms of O–O bonds, at high pressures, the SiO_x units with $x \geqslant 6$ are dominant. The mean bond length Si–O in those units decreases. The value of the first peak position of O-Si–O bond angle distribution in SiO_7 units is smaller than in SiO_6 units and higher than in SiO_8 units (see appendix - figure A·2). In addition, there is a tight relation between PRDF and bond angle distribution [26]. Hence, the mean O–O bond length also decreases significantly under compression.

Figure 5 shows the change in the fraction of SiO_x ($x \geqslant 4$) units. At 0 GPa, SiO_4 accounts for about 75%, SiO_5 is about 20%, and the rest is mostly SiO_3. SiO_x units with $x \geqslant 6$ are then almost non-existent in the system. The formation of SiO_3 and SiO_5 in $MgSiO_3$ at 0 GPa is due to doping MgO [41]. The ratio of SiO_x units varies drastically with pressure. Specifically, the proportion of SiO_4, SiO_5, SiO_6, and SiO_7 units alternately account for the highest proportion at pressures from 0 to 6 GPa, 6 to 27 GPa, 27 to 125 GPa and from 125 onwards. The

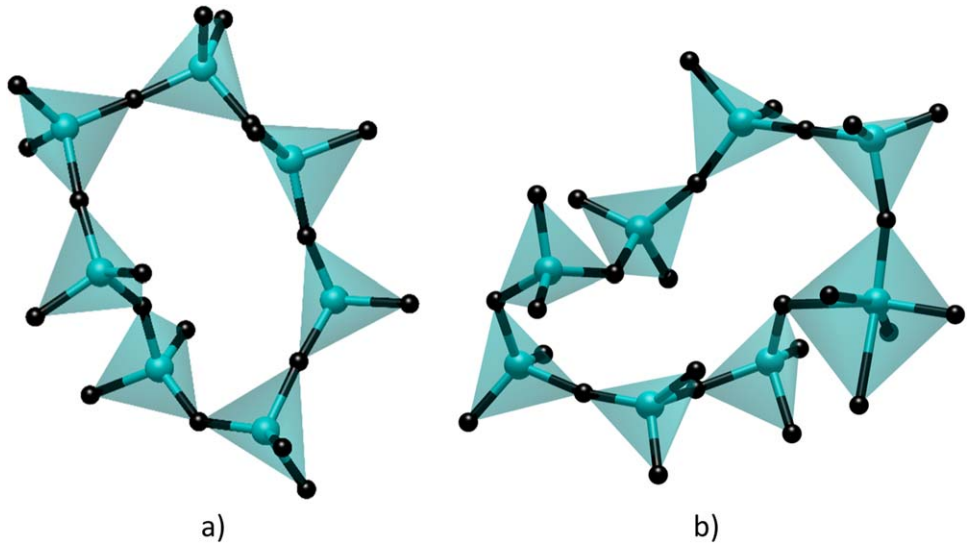

Figure 2. Ring visualization. (a) 7-fold Si ring at 0 GPa. (b) 8-fold Si ring at 0 GPa. The atoms are color-coded. Back rigid spheres are O species, cyan ones represent Si atoms.

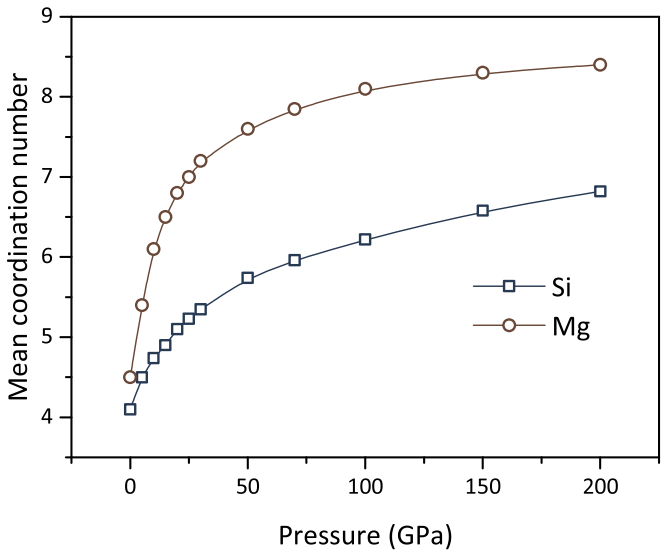

Figure 3. The mean coordination number of Si and Mg under compression in $MgSiO_3$ at 3000 K.

proportion of SiO_5, SiO_6 and SiO_7 units has a peak at 14, 62 and 175 GPa, respectively. At 200 GPa, SiO_4 and SiO_5 units virtually disappear while SiO_7 are primary units. Figure 6 visually shows the evolution as well as the spatial distribution of the SiO_x and MgO_y structural units at the pressures of 0, 50, 100 and 200 GPa. At 200 GPa, MgO_y with $y \geqslant 6$ dominates the system.

3.2 Ring analysis

The ring analysis is carried out to somewhat clarify the IRO in $MgSiO_3$. Figure 7 shows the ring statistics (or ring size distribution) of Si–O and T–O (T is Mg or Si) in $MgSiO_3$ from 0 to 200 GPa. The fraction of rings is calculated based on the number of certain rings over the total number of rings of sizes from 2 to 11. There are large Si–O rings because the -Si–O- network is deformed and broken when doping MgO [50]. The – ring statistics has the gaussian-like form for all pressures while the Si–O ring statistics has that form only at 0 GPa. Therefore – rings are more topologically ordered than Si–O rings. The changing of Si–O ring size distribution by pressure is attributed to the effect of Mg atoms on SiO_x polyhedrons and on the -Si–O- network under compression. At ambient pressure, Mg species act as both network former and network modifier or, in the other words, intermediate roles. The influence of Mg on the network at high pressure could be stronger than at low

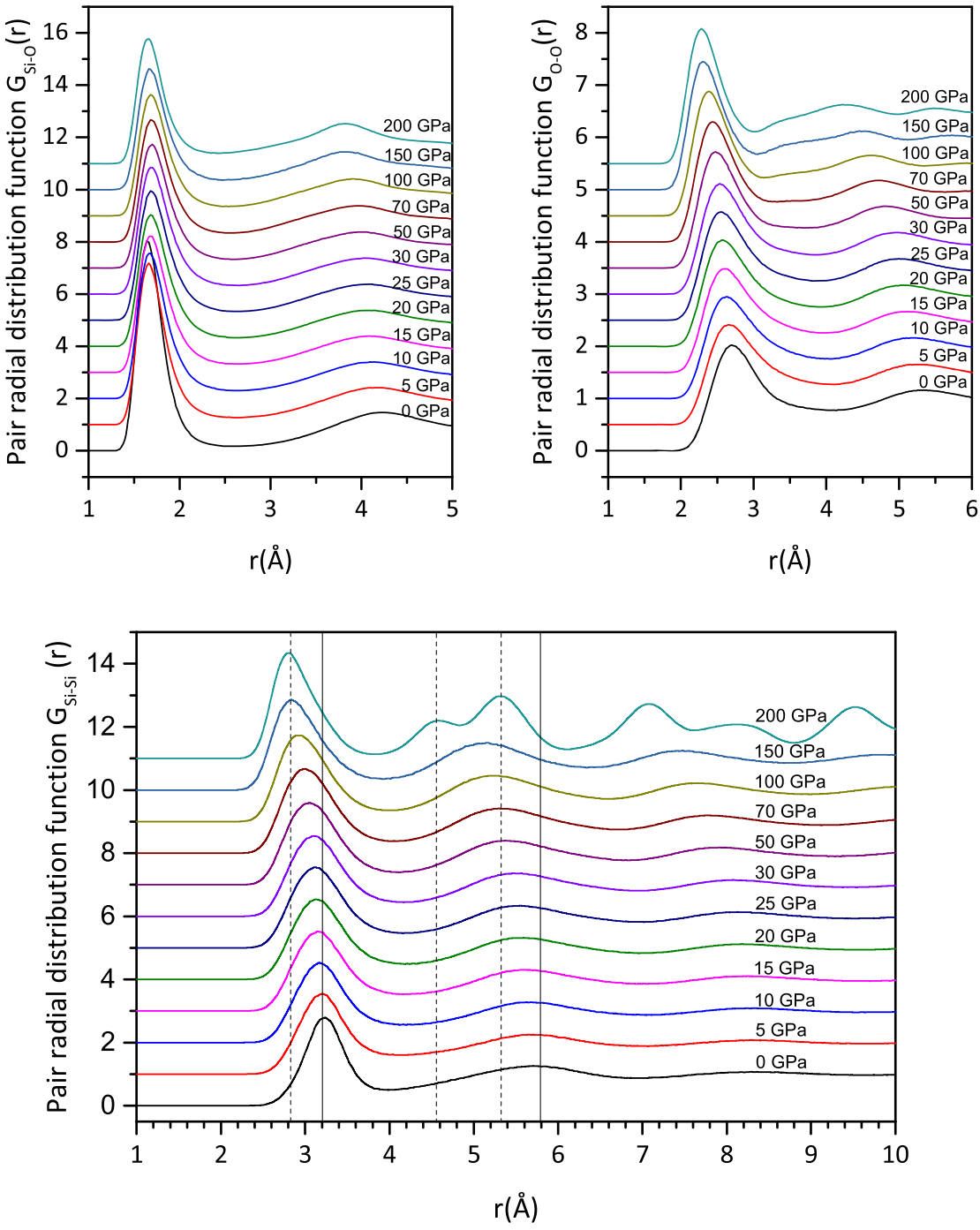

Figure 4. PRDFs of α and β species (α and β are O and Si) under compression.

pressure. The Mg species would break the short paths connecting two Si atoms. Therefore, the ring statistics are not in the gaussian shape at pressures above 0 GPa.

In the case of the – ring, at ambient pressure, the 4- and 5-fold rings account for around 24% and these results. The 6-fold, 7-fold and 8-fold rings are around 15.2%, 6.2% and 2.2%, respectively. At higher pressures, the ring size distribution shifts to the left. From 50 GPa, the 3-fold ring accounts for the highest proportion, it is even more than 50% at pressure higher than or equal 100 GPa. Besides, the large rings (size $\geqslant 6$) almost vanish at high pressure. At 200 GPa, the fraction of the 5-fold ring is about 3%. Under compression, the mean coordination number of Si and Mg increased (see figure 3). Atoms are more tightly packed. Therefore, the percentages of small T–O rings increasingly rise, and the percentages of large – rings go down. For Si–O rings, there is a massive change in the ring statistics under compression. At 0 GPa, the Si–O ring statistic has a gaussian form, with a peak at 5-fold. Paradoxically, when the pressure increases and reaches 20 GPa, the 5-fold ring has the lowest proportion. The 11-fold ring which has the lowest proportion at 0 GPa now is dominant. As the

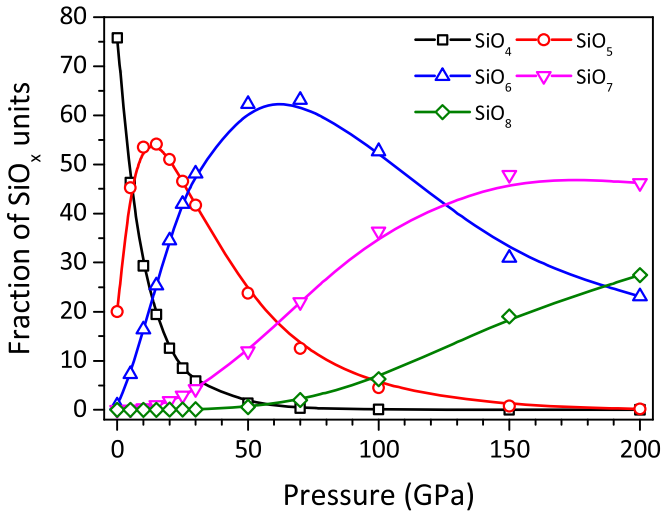

Figure 5. The change in the fraction of SiO_x units under compression.

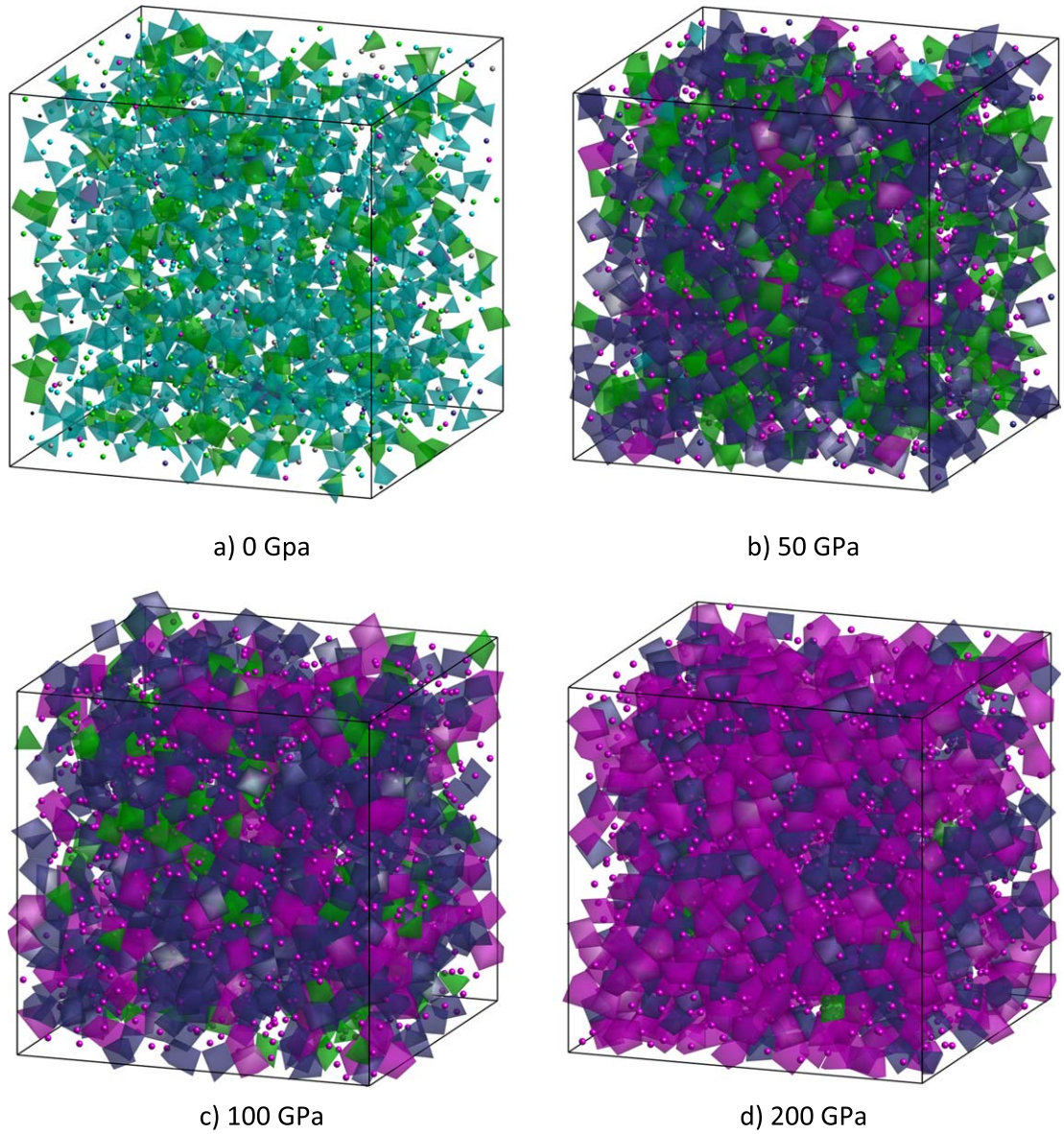

Figure 6. Visualization of Mg and Si coordination number of the models at different pressures. The Mg atoms (big spheres), 3-coordinated Si atoms (small spheres), and Si–O coordinated polyhedron are color-coded to denote the coordination number, where black/gray represents threefold, cyan for fourfold, green for fivefold, dark blue for sixfold and magenta for sevenfold or higher.

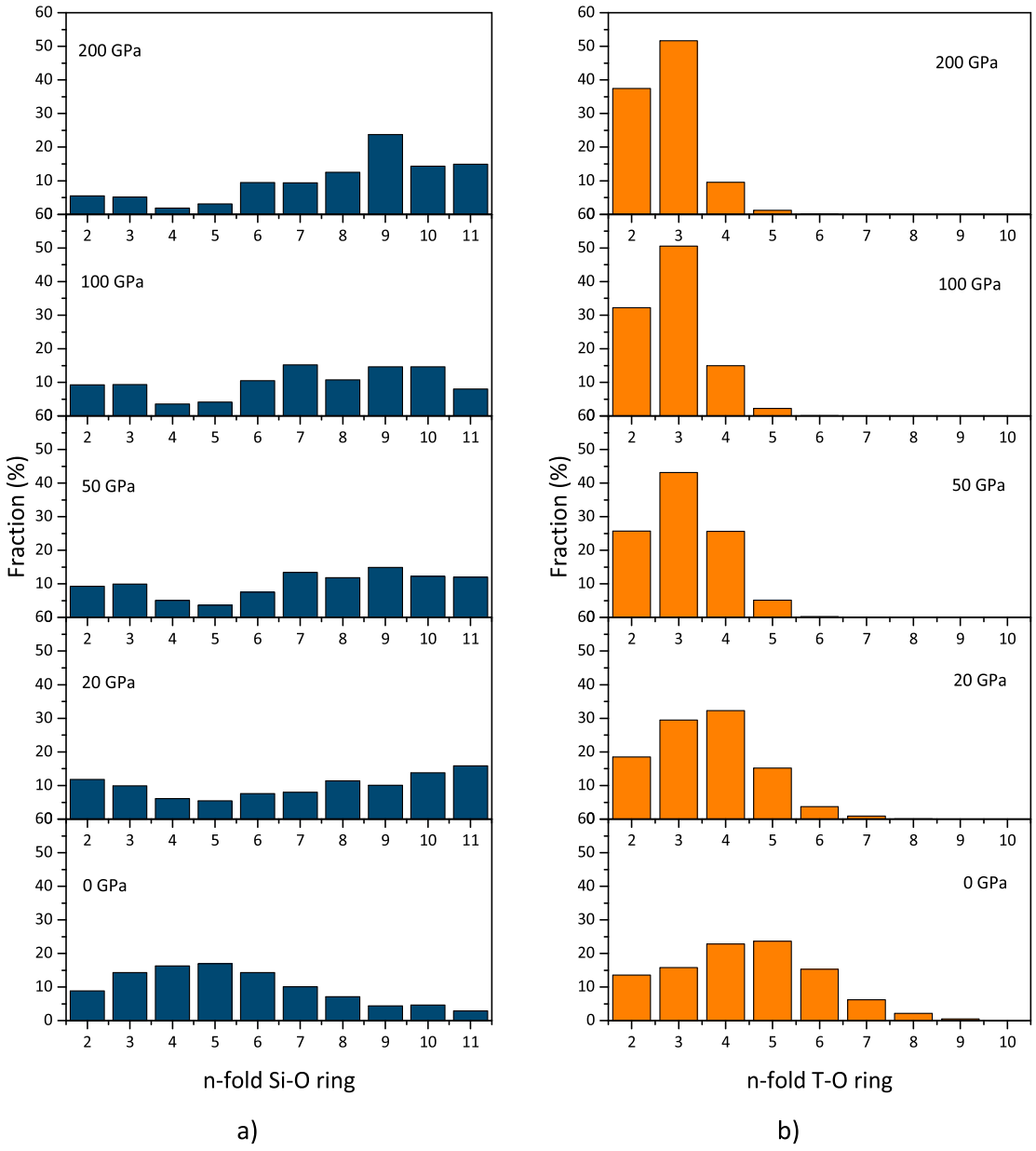

Figure 7. Ring statistics at different pressures. (a) n-fold Si–O ring, (b) n-fold – ring.

pressure increases further, the ring statistics continue changing significantly but 4- and 5-fold rings still account for the smallest ratio. This shows the strong influence of pressure on the structure of the Si–O network. At 200 GPa, the 9-fold ring fraction is surprisingly higher than others. This will affect the intermediate range order of the -Si–O- network. In particular, we use that phenomenon to explain the splitting peak of the second peak in Si–Si PRDF.

For convenience, we consider the distribution of bond length from a Si atom on a ring to the nearest second one on the same ring as the Si–Si-Si distance distribution. The Si–Si-Si distance distribution depends very strongly on certain rings (see figure 8). The 4-fold, 5-fold and 6-fold rings have a gaussian form distribution, with peaks at 4.1, 4.8 and 4.7 Å, respectively. The Si–Si-Si distance distribution has a narrower full width at half maximum (FWHM) on 4-fold rings than the ones on 5-fold rings and 6-fold rings. The Si–Si-Si distance distribution of 10 and 11-fold rings varies significantly compared to the small rings. Therefore, large rings are very topologically flexible. Large rings are constructed by many Si–O paths. The SiO_x units on large rings have more ability to arrange than on small rings with a constraint minimizing the cohesive energy of the whole configuration. Conversely, low-fold rings, typically 2-fold and 3-fold rings, are formed by stretching Si–O bond length, bending of Si–O-Si and O-Si–O bond angle to optimize the raised energy [27]. The smaller the rings are, the more the rings are affected by the energy constraint. Compared to small-size rings, higher-fold ones have more varied shapes. Hence, Si–Si-Si distance distribution in large rings does not have the Gaussian shape.

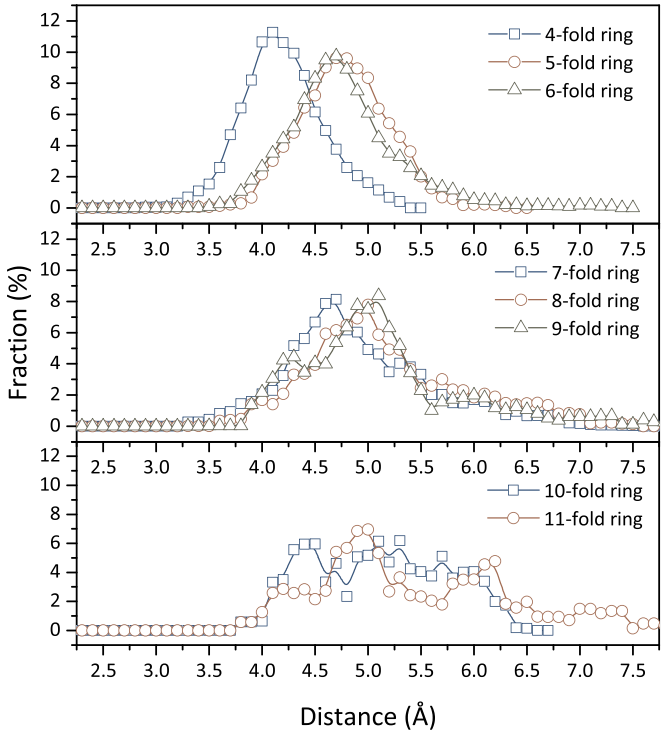

Figure 8. Si–Si-Si distance distribution on different types of rings at 200 GPa.

Although the distance distribution of Si–Si-Si of the 9-fold ring is asymmetric, it has a sharp peak at about 5.3 Å. Ring size distribution, as shown in figure 7, indicates that at 200 GPa, 9-fold rings are enormous in proportion compared to others. The 9-fold ring proportion is almost 24% while the second most dominant one is the 11-fold ring which accounts for only about 15%. The combination of the dominance in the ratio and the high peak position of Si–Si-Si distance distribution of the 9-fold ring regulates Si–O PRDF. The second peak of Si–Si PRDF tends to shift to the left under compression (see figure 4), and at 200 GPa, the second peak splits into two subpeaks. The first subpeak is at about 4.6 Å while the second one is at about 5.3 Å. Based on the above analysis, the phenomenon that the second peak splits into two small subpeaks at 200 GPa is attributed to the massive formation of 9-fold rings. The small subpeak corresponds to the reduction of averaged bond length among interactive atoms (similar to the cases in pressure range beneath 200 GPa). The high subpeak is ascribed to the position of the sharp peak in Si–Si-Si distance distribution.

Figure 9 demonstrates the Q^n distributions of rings under compression to have a better understanding of rings. At 0 GPa, Q^n distribution of 2-, and 3- fold rings have peaks at $n = 4$ (see figure 9(a)). On 2-fold rings, the value of Q^3 is close to the value of Q^5, about 27%. The fraction of Q^4 in 2-fold rings is higher than the one in other rings. For rings of size 4 or higher, Q^3 accounts for the highest proportion. Q^n has almost the same distribution across the different rings at the same pressure, except for the distribution of Q^n on the 11-fold ring at 100 GPa (see figure 9(c)). The peak shift of Q^n distribution from 3 or 4 at ambient pressure to 6 or 7 at pressure of 50 GPa or higher indicates that rings tend to merge under compression.

3.3 Mg-rich region

The ring statistical analysis can also explain the heterogeneity of $MgSiO_3$. When large rings are formed on the -Si–O- network, inside those large rings there is no silicon atom because there is no shortcut path [47]. Therefore, the domain inside the large ring will have a high density of oxygen atoms creating a negative charge region (see figure 10(a)). The Mg^{2+} ions will therefore be attracted inward to neutralize the charge (see figure 10(b)) forming an Mg-rich region. The spatial distribution of Mg^{2+} ions is not uniform, leading to the heterogeneity of the material. As the pressure increases, the greater the proportion of large Si–O rings appears (see ring statistics in figure 7(a)), the higher the ability to capture Mg atoms. In other words, the heterogeneity of $MgSiO_3$ increases with pressure.

3.4 Voronoi

The Si- and O-Voronoi volume distributions on the rings are also analyzed to explain the arrangement of atoms on the -Si–O- network. Figure 11 shows the change in the volume of the Voronoi on particular rings with

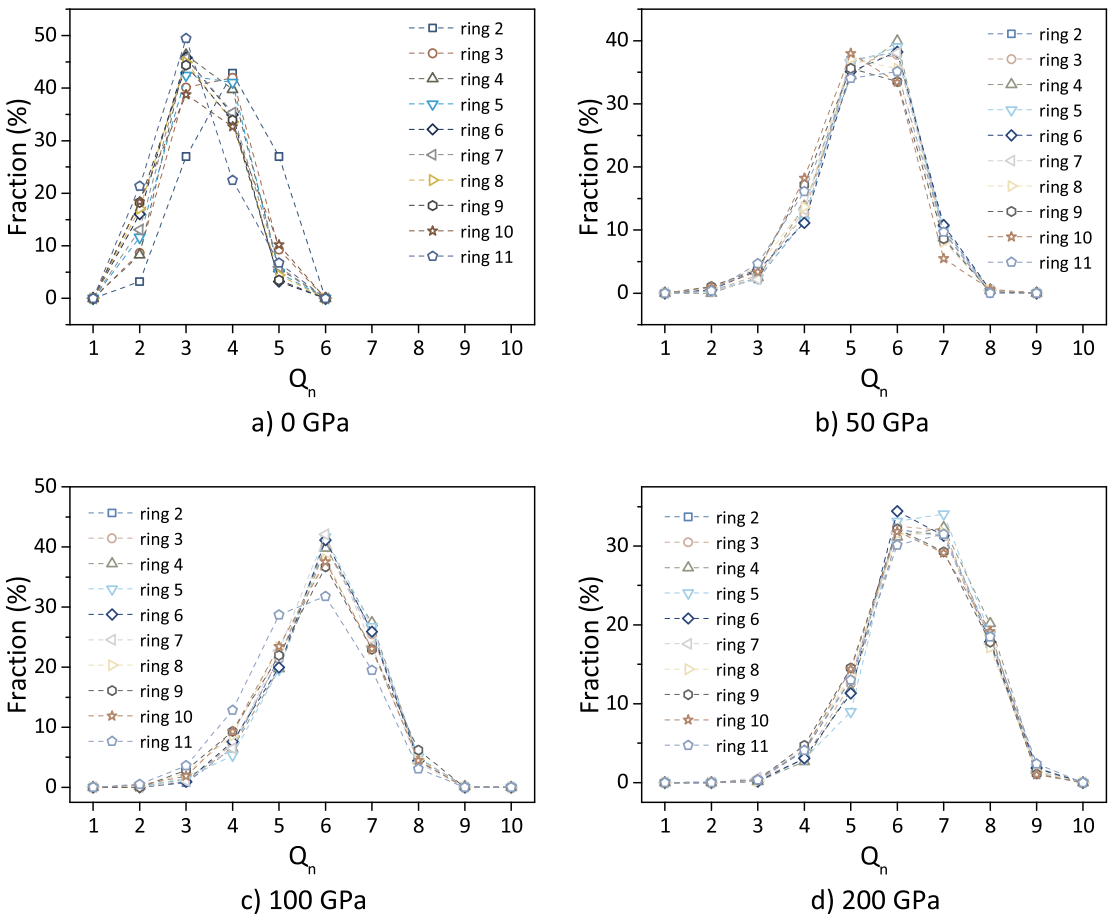

Figure 9. Q^n distribution of different ring sizes at different pressures.

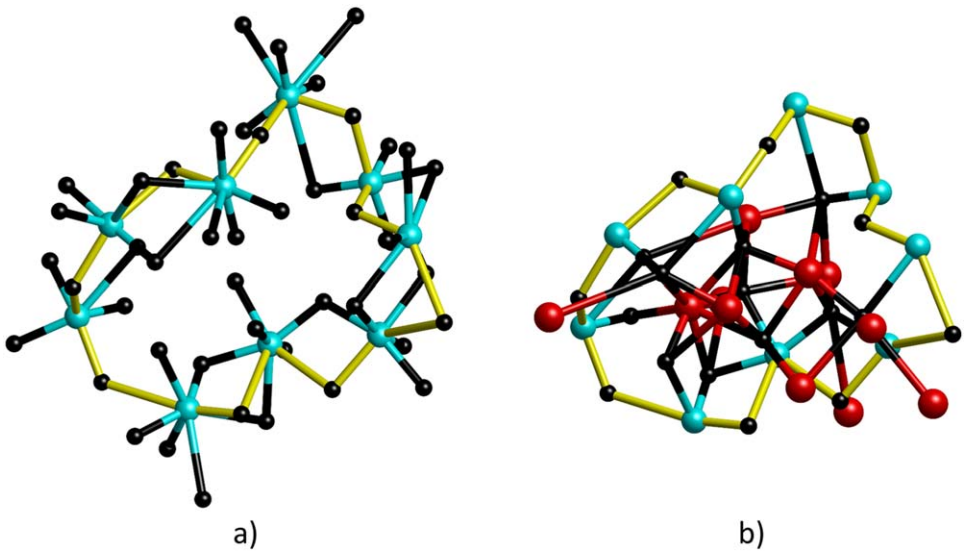

Figure 10. Cyan, black and red spheres are Si, O and Mg atoms respectively, the yellow path is 10-fold ring. (a) Ring with surrounding oxygen atoms. (b) Mg-rich region inside the ring

pressure. Figure 12 is an example of Si and O-Voronoi on 6-fold ring at pressures of 50 and 200 GPa, and the spatial distribution of Voronoi on the 6-fold is shown in figure 13. At 0 GPa, the Si-voronoi volume ranges from 7.50 to 7.76 $Å^3$. In contrast, at ambient pressure, O-Voronoi are strongly dependent on ring type and have a much larger volume than Si-voronoi. At 0 GPa, the volume of O increases from about 13 $Å^3$ to almost 16 $Å^3$, as the ring size increases from 2 to 6. However, with rings having size greater than 6, the larger the ring size, the

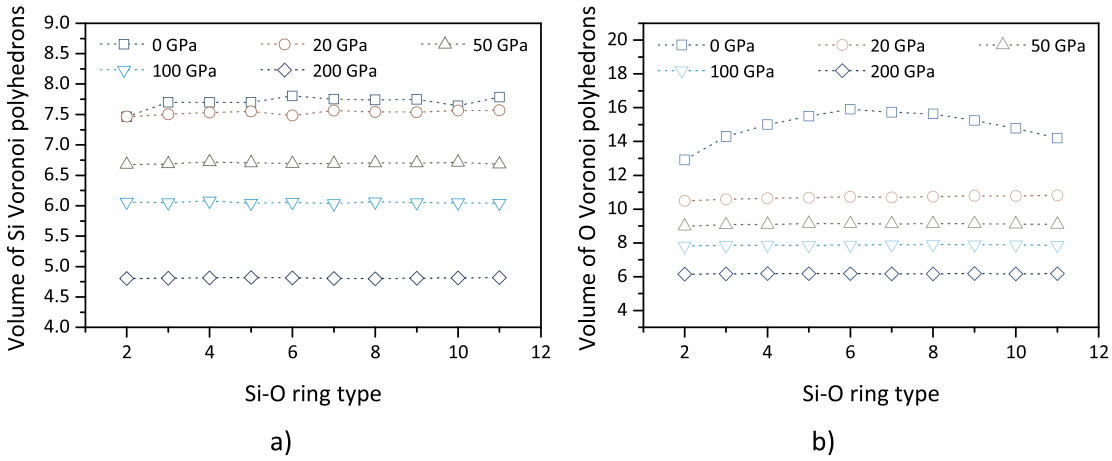

Figure 11. Characteristic of Voronoi polyhedrons of rings: average volume of Si-Voronoi (a) and O-Voronoi (b) on rings under compression.

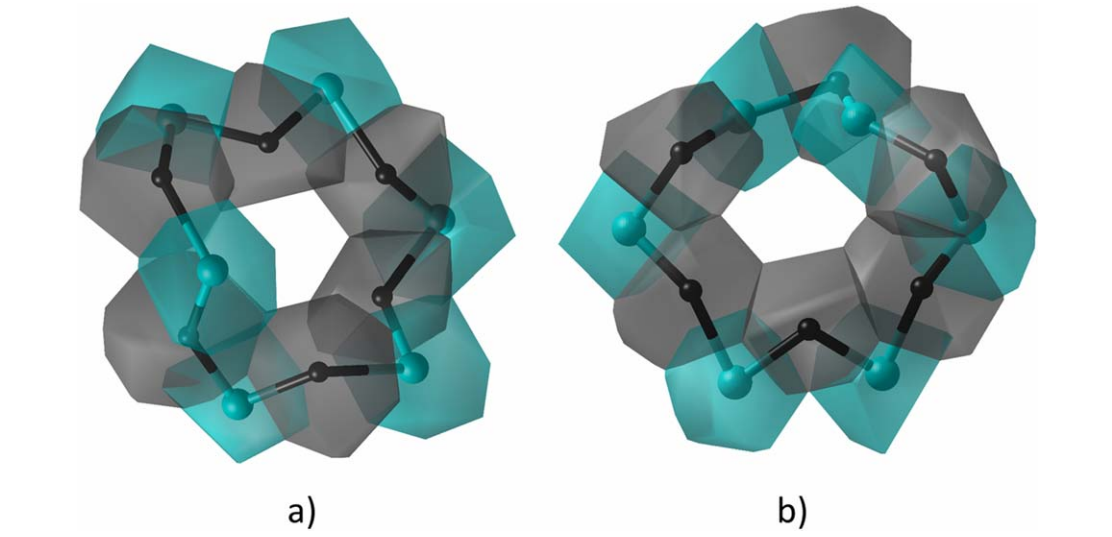

Figure 12. Voronoi on rings. (a) 6-fold ring at 50 GPa. (b) 6-fold ring at 200 GPa. Cyan and gray polyhedrons correspond for Voronoi centered by Si and O atoms.

smaller the O-Voronoi volume. With the 11-fold ring, the O-Voronoi volume is about 14.3 $Å^3$. The change of O-Voronoi volume with the size of the ring is attributed to the distortion of the SiO_x units and the arrangements of those units on the ring. At ambient pressure, the O-Si–O bond angle distribution has a peak at about 109° [12]. Geometrically, rings that are small in size will have a smaller internal O-Si–O angle in SiO_x than 109°. The smaller the ring, the more distorted the SiO_x units are. In addition to the distorting effect of SiO_x units, the arrangement of SiO_x units on rings via shared Si atoms also affects the volume of the O-Voronoi. The O-centered Voronoi volume of small rings (size $\leqslant 5$) is mainly affected by the distortion of SiO_4 units. For the larger rings, the atoms are more flexible to arrange to form highly symmetric SiO_x units, which helps to reduce the energy of the system [27]. This means that the SiO_x units on the large rings (size > 5) have less distortion. There is a relation between Si–O-Si angle and O-Voronoi volume (see figure 11(b) and figure 14). It is noticed that the mean O-Voronoi volume is proportional to the mean angle of Si–O-Si. The fact that mean Si–O-Si angle reaches a value of 148.2° then gradually decreases to 137.5° could correspond to the volume of O-Voronoi decreasing when the ring size is greater than 6. Hence, the mean O-Voronoi volume in 6-fold rings is greater than the ones in other rings.

At pressures of 20 GPa or more, the mean Voronoi volumes of atoms of the same type on different rings have almost the same value. The Si atoms are surrounded by O atoms, while the O atoms are bonded to both Mg and Si atoms. Besides, the mean Si–O bond length is shorter than the mean Mg–O bond length at the same pressure condition [17]. The average distance from the center point of Si-Voronoi is then shorter than the one of O-voronoi. Thus, the O-Voronoi would have a larger volume than the Si-Voronoi. Specifically, at pressures at

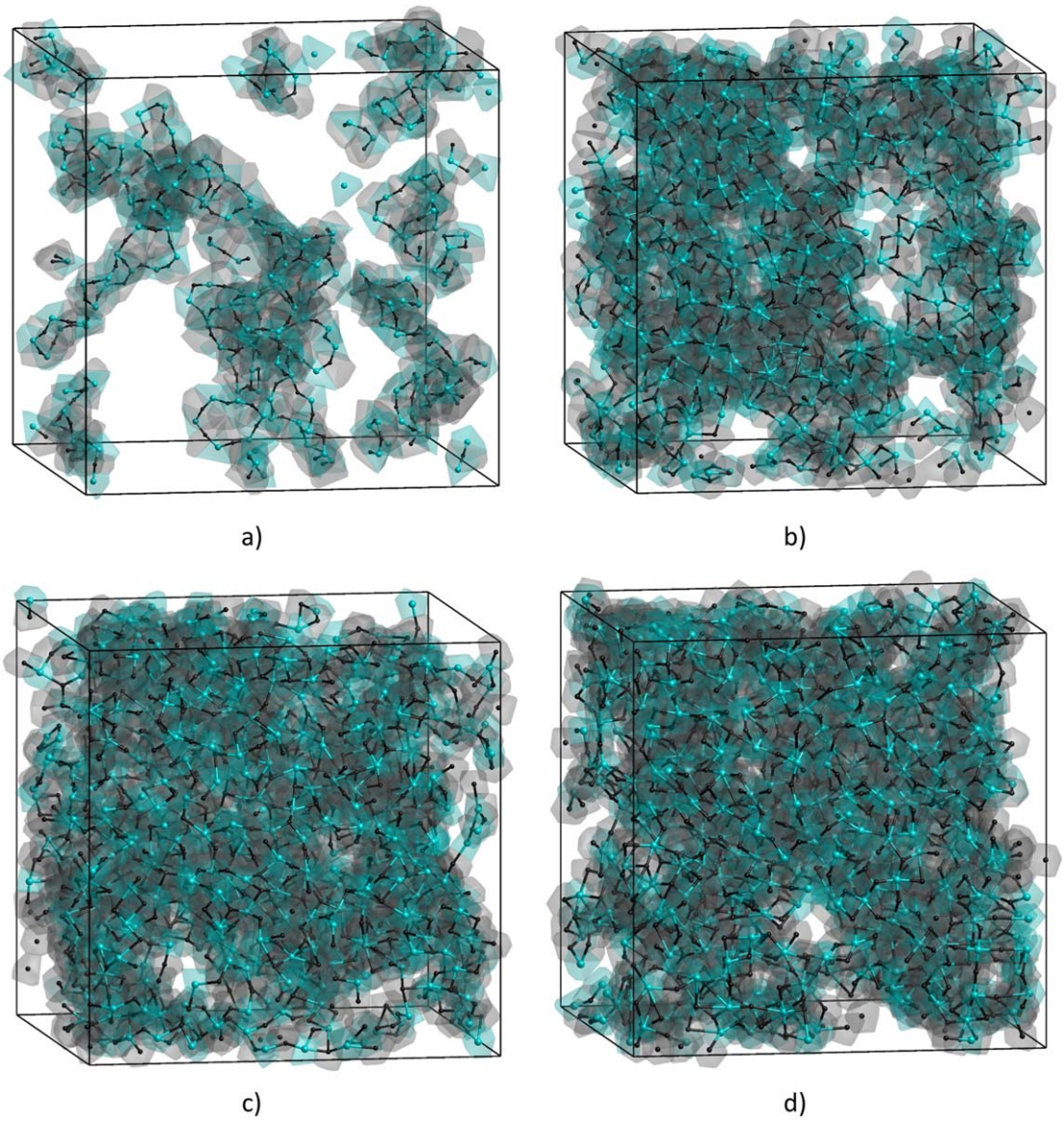

Figure 13. The snapshot of Voronoi of 6-fold Si–O rings at (a) 0 GPa, (b) 50 GPa, (c) 100 GPa, (d) 200 GPa.

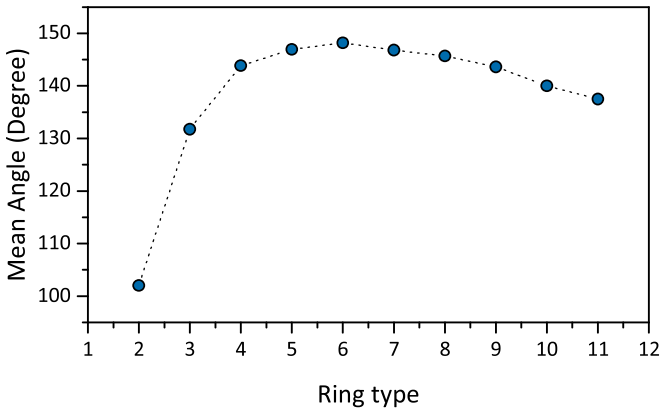

Figure 14. The mean Si–O-Si angle on rings at 0 GPa.

50, 100 and 200 GPa, the Si-Voronoi volume is 6.7, 6.1, 4.8 $Å^3$ while the O-Voronoi volume is 9.0, 7.8 and 6.0 $Å^3$, respectively. As the pressure increases, the number of edge-sharing and face-sharing bonds increases (see appendix - table A1), the size of the model decreases due to compression, and the polymerization of the -Si–O-

network increases. The atoms will be tightly packed together, and the rings connect to others or even overlap (for example, 2-fold rings overlap a 10-fold ring in figure 10(a) and 6-fold rings merge under compression in figure 13). Therefore, Voronoi of the same type on different rings have the same average volume.

4 Conclusion

We conduct a study on the local structural change and intermediate-range order of $MgSiO_3$ liquid at 3000 K under compression. The Si–Si and O–O PRDFs rapidly change by pressure while the Si–O PRDF is quite stable, because of the formation of edge- and face-sharing linkages as well as the increase in the mean coordination number of Si. At 200 GPa, the 9-fold rings dominate the system, Si–Si-Si distance distribution on 9-fold rings has a sharp peak at around 5.3 Å and Si–O linkages shrink due to high pressure. This infers the splitting peak of Si–Si PRDF into 2 subpeaks at 4.6 Å and 5.3 Å. The formation of large rings, at high pressures, sheds light on the formation of Mg-rich regions. In particular, the O atoms inside the large rings and there is no shortcut path which contains Si species. They would generate a high negative charge domain, attracting the Mg^{2+} ions and forming Mg-rich regions. The non-uniform distribution of Mg in space leads to the heterogeneity of the $MgSiO_3$. In terms of Voronoi analysis, our results indicate that at ambient pressure, the mean Si-Voronoi volume is in the range of 7.5–7.8 $Å^3$ on different types of rings. The mean O-Voronoi volume increases from about 13.0 $Å^3$ on 2-fold ring to nearly 16.0 $Å^3$ on 6-fold ring, then decreases to 14.3 $Å^3$ on 11-fold ring. This phenomenon is attributed to the topological distortion of SiO_4 units of small rings, the mean Si–O-Si angle and the way SiO_x units arrange on large rings.

Acknowledgments

This simulation is carried out on the high-performance computing system in RIKEN. Representative laboratory at RIKEN: RIKEN Cluster for Pioneering Research, Theoretical Quantum Physics Laboratory and RIKEN Center for Computational Science, Discrete Event Simulation Research Team.

This research is performed with the support of Hanoi University of Science and Technology, and Politecnico di Torino.

Data availability statement

All data that support the findings of this study are included within the article (and any supplementary files).

Appendix

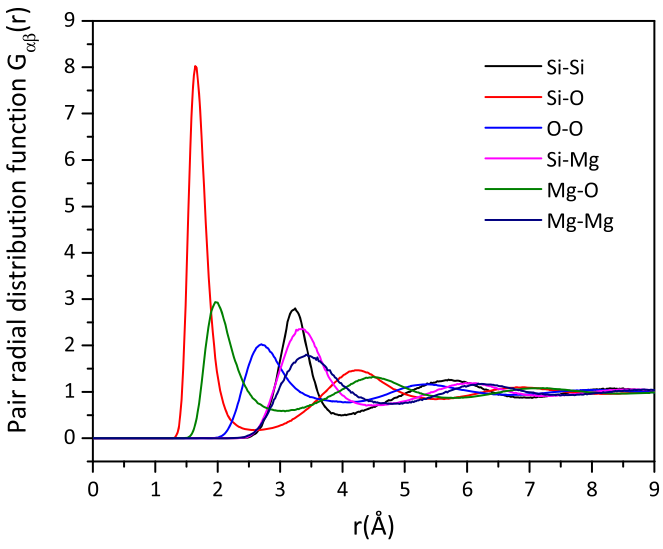

Figure A1. The PRDF of Si–Si, Si–O, O–O, Si–Mg, Mg–O, Mg-Mg at ambient pressure.

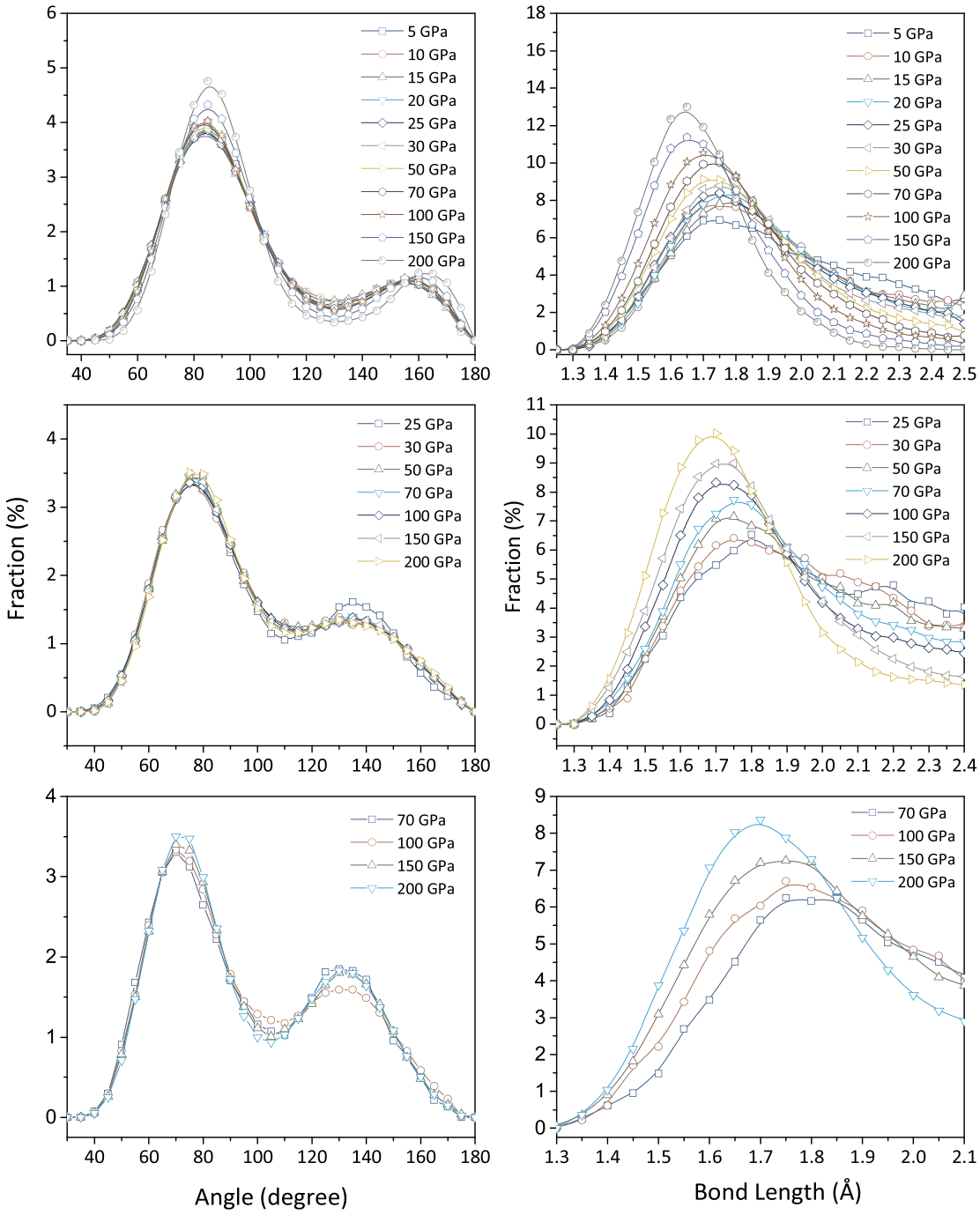

Figure A2. The bond angle distribution (left) and bond length distribution within each type of SiO_x ($x = 6, 7, 8$) units.

Table A1. The number of corner-(N_c), edge-(N_e), face-sharing (N_f) network per the number of Si atoms at different pressure, corresponding with the mean bond length of them, corner-(CSBL), edge-(ESBL), face-sharing bond length (FSBL).

Pressure (GPa)	N_c	N_e	N_f	CSBL	ESBL	FSBL
0	1.27	0.1	0.00	3.31	2.91	*NaN*
5	1.48	0.24	0.01	3.33	2.97	2.82
10	1.60	0.33	0.02	3.33	2.97	2.76
15	1.71	0.40	0.02	3.34	2.97	2.75
20	1.76	0.49	0.04	3.34	2.95	2.71
25	1.79	0.58	0.06	3.34	2.95	2.79
30	1.82	0.64	0.05	3.34	2.97	2.74
50	1.97	0.83	0.09	3.35	2.95	2.73
70	2.06	0.94	0.13	3.33	2.94	2.76
100	1.96	1.15	0.22	3.32	2.93	2.73
150	1.83	1.42	0.36	3.35	2.89	2.73
200	1.58	1.76	0.43	3.28	2.88	2.71

ORCID iDs

Hoang Anh Nguyen https://orcid.org/0000-0002-7504-5284
Nguyen Van Hong https://orcid.org/0000-0002-0097-9840

References

[1] Bykova E *et al* 2018 Metastable silica high pressure polymorphs as structural proxies of deep earth silicate melts *Nat. Commun.* **9** 4789
[2] Karki B B and Stixrude L P 2010 Viscosity of $MgSiO_3$ liquid at Earth's mantle conditions: implications for an early magma ocean *Science (80-.).* **328** 740–2
[3] Sakai T, Dekura H and Hirao N 2016 Experimental and theoretical thermal equations of state of $MgSiO_3$ post-perovskite at multi-megabar pressures *Sci Rep.* **6** 6–13
[4] Sen S, Maekawa H and Papatheodorou G N 2009 Short-range structure of invert glasses along the pseudo-binary join $MgSiO_3$-Mg2SiO_4: results from 29Si and 25Mg MAS NMR spectroscopy *J. Phys. Chem. B* **113** 15243–8
[5] Kohara S *et al* 2004 Glass formation at the limit of insufficient network formers *Science (80-.).* **303** 1649–52
[6] Al-Hasni B M and Mountjoy G 2014 A molecular dynamics study of the atomic structure of x(MgO) 100 - X(SiO2) *J. Non. Cryst. Solids* **400** 33–44
[7] Van Yen N, Plan E L C V M, Kien P H, Nguyen A T, Van Hong N and Phan H 2022 Topological structural analysis and dynamical properties in MgSiO3 liquid under compression *Eur. Phys. J. B* **95** 1–11
[8] Kubicki J D and Lasaga A C 1991 Molecular dynamics simulations of pressure and temperature effects on $MgSiO_3$ and Mg_2SiO_4 melts and glasses *Phys. Chem. Miner.* **17** 661–73
[9] Salmon P S *et al* 2019 Pressure induced structural transformations in amorphous $MgSiO_3$ and $CaSiO_3$ *J. Non-Crystalline Solids X* **3** 100024
[10] Wilding M C, Benmore C J and Weber J K R 2010 Changes in the local environment surrounding magnesium ions in fragile MgO-SiO_2 liquids *EPL* **89** 1–5
[11] Spera F J, Ghiorso M S and Nevins D 2011 Structure, thermodynamic and transport properties of liquid $MgSiO_3$: comparison of molecular models and laboratory results *Geochim. Cosmochim. Acta* **75** 1272–96
[12] Haskins J B, Stern E C, Bauschlicher C W and Lawson J W 2019 Thermodynamic and transport properties of meteor melt constituents from *ab initio* simulations: $MgSiO_3$, SiO2, and MgO *J. Appl. Phys.* **125** 235102
[13] de Koker N P, Stixrude L and Karki B B 2008 Thermodynamics, structure, dynamics, and freezing of Mg_2SiO_4 liquid at high pressure *Geochim. Cosmochim. Acta* **72** 1427–41
[14] Lan M T, Duong T T, Huy N V and Van Hong N 2017 Network structure of SiO_2 and MgSiO3 in amorphous and liquid States *Mater. Res. Express* **4** 035202
[15] Wilding M C, Benmore C J and Weber J K R 2008 *In situ* diffraction studies of magnesium silicate liquids *J. Mater. Sci.* **43** 4707–13
[16] Adjaoud O, Steinle-Neumann G and Jahn S 2008 Mg_2SiO_4 liquid under high pressure from molecular dynamics *Chem. Geol.* **256** 185–92
[17] San L T, Van Hong N, Iitaka T and Hung P K 2016 Structural organization, micro-phase separation and polyamorphism of liquid $MgSiO_3$ under compression *Eur. Phys. J. B* **89** 73
[18] Cormier L and Cuello G J 2011 Mg coordination in a MgSiO3 glass using neutron diffraction coupled with isotopic substitution *Phys. Rev. B - Condens. Matter Mater. Phys.* **83** 1–8
[19] Lin C C, Chen S F, Gun Liu L and Li C C 2007 Anionic structure and elasticity of Na2O-MgO-SiO_2 glasses *J. Non. Cryst. Solids* **353** 413–25
[20] Wang Y *et al* 2014 Atomistic insight into viscosity and density of silicate melts under pressure *Nat. Commun.* **5** 1–10
[21] Son N H and Anh N H 2020 Structural simulation of Mg_2SiO_4 under compression *Struct. Simul. Mg2SiO4 under Compression* **36** 18–28
[22] Yi Y S, Khim H, Kim Y H and Lee S K 2021 Spectral proxies for bonding transitions in SiO2 and MgSiO3 polymorphs at high pressure up to 270 GPa by O K -edge x-ray Raman scattering *Phys. Rev. B* **103** 26–37
[23] Panero W R, Akber-Knutson S and Stixrude L 2006 Al_2O_3 incorporation in $MgSiO_3$ perovskite and ilmenite *Earth Planet. Sci. Lett.* **252** 152–61
[24] Kohara S and Suzuya K 2005 Intermediate-range order in vitreous SiO_2 and GeO_2 *J. Phys. Condens. Matter* **17** S77

[25] Nguyen T T, Nguyen T T, Dinh H T and Le V V 2019 Molecular dynamics simulations of structural and mechanical properties in $MgSiO_3$ glass *Phys. Status Solidi Basic Res.* **256** 1–9
[26] Son N H, Anh N H, Kien P H, Iitaka T and Van Hong N 2020 Topology of SiOx-units and glassy network of magnesium silicate glass under densification: correlation between radial distribution function and bond angle distribution *Model. Simul. Mater. Sci. Eng.* **28** 065007
[27] Kalia R K, Nakano A and Vashishta P 1993 Structure of rings in vitreous SiO_2 *Phys. Rev. B* **47** 3053–62
[28] Cormier L and Cuello G J 2013 Structural investigation of glasses along the $MgSiO_3$-$CaSiO_3$ join: diffraction studies *Geochim. Cosmochim. Acta* **122** 498–510
[29] Karki B B 2018 First-principles molecular dynamics simulations of silicate melts: structural and dynamical properties *Theor. Comput. Methods Miner. Phys. Geophys. Appl.* **71** 355–89
[30] Karki B B, Bhattarai D and Stixrude L 2007 First-principles simulations of liquid silica: structural and dynamical behavior at high pressure *Phys. Rev. B - Condens. Matter Mater. Phys.* **76** 9–13
[31] Trave A, Tangney P, Scandolo S, Pasquarello A and Car R 2002 'Pressure-induced structural changes in liquid SiO_2 from *Ab Initio* simulations *Phys. Rev. Lett.* **89** 1–4
[32] Stixrude L and Bukowinski M S T 1991 Atomic structure of SiO_2 glass and its response to pressure *Phys. Rev. B* **44** 2523–34
[33] Liu Y, Bai C, Lv X and Wei R 2015 Molecular dynamics simulation on the influence of Al_2O_3 on the slag structure at 1873 K *Mater. Today Proc.* **2** S453–9
[34] Kohara S *et al* 2011 Relationship between topological order and glass forming ability in densely packed enstatite and forsterite composition glasses *Proc. Natl. Acad. Sci. U. S. A.* **108** 14780–5
[35] Oganov A R, Brodholt J P and Price G D 2000 Comparative study of quasiharmonic lattice dynamics, molecular dynamics and debye model applied to MgSiO3 perovskite *Phys. Earth Planet. Inter.* **122** 277–88
[36] Nevins D, Spera F J and Ghiorso M S 2009 Shear viscosity and diffusion in liquid MgSiO3: Transport properties and implications for terrestrial planet magma oceans *Am. Mineral.* **94** 975–80
[37] Liu Z J, Zhang C R, Sun X W, Hu J B, Song T and Chu Y D 2011 The melting curve of MgSiO3 perovskite from molecular dynamics simulation *Phys. Scr.* **83** 045602
[38] Goryaeva A M, Carrez P and Cordier P 2017 Modeling defects and plasticity in $MgSiO_3$ post-perovskite: Part 3—screw and edge [001] dislocations *Phys. Chem. Miner.* **44** 521–33
[39] Funamori N and Yamamoto S 2004 Exploratory studies of silicate melt structure at high pressures and temperatures by *in situ* x-ray diffraction *J. Geophys. Res.* **109** 1–8
[40] Wilding M C, Benmore C J, Tangeman J A and Sampath S 2004 Evidence of different structures in magnesium silicate liquids: coordination changes in forsterite- to enstatite-composition glasses *Chem. Geol.* **213** 281–91
[41] Matsui Y and Kawamura K 1980 Instantaneous structure of an $MgSiO_3$ melt simulated by molecular dynamics *Nature* **285** 648–9
[42] King S V 1967 Ring configurations in a random network model of vitreous silica *Nature* **213** 1112–3
[43] Taniguchi T, Okuno M and Matsumoto T 1997 X-ray diffraction and EXAFS studies of silicate glasses containing Mg, Ca and Ba atoms *J. Non. Cryst. Solids* **211** 56–63
[44] Wooten F 2002 Structure, odd lines and topological entropy of disorder of amorphous silicon *Acta Crystallogr., Sect. A: Found. Crystallogr.* **58** 346–51
[45] Goetzke K and Klein H J 1991 Properties and efficient algorithmic determination of different classes of rings in finite and infinite polyhedral networks *J. Non. Cryst. Solids* **127** 215–20
[46] Yuan X and Cormack A N 2002 Efficient algorithm for primitive ring statistics in topological networks *Comput. Mater. Sci.* **24** 343–60
[47] Matsumoto M, Baba A and Ohmine I 2007 Topological building blocks of hydrogen bond network in water *J. Chem. Phys.* **127** 134504
[48] Franzblau D S 1991 Computation of ring statistics for network models of solids *Phys. Rev. B* **44** 4925–30
[49] Guttman L 1990 Ring structure of the crystalline and amorphous forms of silicon dioxide *J. Non. Cryst. Solids* **116** 145–7
[50] Tangeman J A, Phillips B L, Navrotsky A, Weber J K R, Hixson A D and Key T S 2001 Vitreous forsterite (Mg_2SiO_4): synthesis, structure, and thermochemistry *Geophys. Res. Lett.* **28** 2517–20